Mid-infrared supercontinuum generation in silicon-germanium all-normal dispersion waveguides

Milan Sinobad, Alberto Dellatorre, Remi Armand, Barry Luther-Davies, Pan Ma, Stephen Madden, Arnan Mitchell, David Moss, Jean-Michel Hartmann, Jean-Marc Fedeli, et al.

Optics Letters

Mid-infrared supercontinuum generation in silicon-germanium all-normal dispersion waveguides

Milan Sinobad,[1,*] Alberto DellaTorre,[1] Remi Armand,[1] Barry Luther-Davies,[2] Pan Ma,[2] Stephen Madden,[2] Arnan Mitchell,[3] David J. Moss,[4] Jean-Michel Hartmann,[5] Jean-Marc Fedeli,[5] Christelle Monat,[1] and Christian Grillet[1]

[1]Université de Lyon, Ecole Centrale de Lyon, Institut des Nanotechnologies de Lyon (INL), 69131 Ecully, France
[2]Laser Physics Centre, Australian National University, Canberra, ACT 0100, Australia
[3]School of Engineering, RMIT University, Melbourne, VIC 3001, Australia
[4]Optical Sciences Centre, Swinburne University of Technology, Hawthorn, VIC 3122, Australia
[5]Université Grenoble Alpes and CEA, LETI, 17 Avenue des Martyrs 38054 Grenoble, France
*Corresponding author: milan.sinobad@ec-lyon.fr

Received 8 July 2020; revised 1 August 2020; accepted 1 August 2020; posted 4 August 2020 (Doc. ID 402159); published 4 September 2020

We demonstrate coherent supercontinuum generation spanning over an octave from a silicon germanium-on-silicon waveguide using ∼200 fs pulses at a wavelength of 4 μm. The waveguide is engineered to provide low all-normal dispersion in the TM polarization. We validate the coherence of the generated supercontinuum via simulations, with a high degree of coherence across the entire spectrum. Such a generated supercontinuum could lend itself to pulse compression down to 22 fs.

https://doi.org/10.1364/OL.402159

Mid-infrared (mid-IR) supercontinuum (SC) is an ideal light probe for broadband molecular absorption spectroscopy, as it retains the intensity, directionality, and coherence properties of the laser pump, while having a wide spectral span in the molecule sensitive mid-IR region (between 2.5 to 15 μm). Spectra altered by molecular resonances can be measured using a single photo-detector in a dual-comb spectroscopy scheme [1,2]. Recently, using this approach, Nader *et al.* detected carbonyl sulfide at 5 μm with coherent mid-IR SC from a silicon-based chip [3]. Dual-comb spectroscopy requires high mutual coherence between two interfering combs as well as a high power spectral density. Furthermore, high phase coherence of spectral components separated by an octave is needed to stabilize the SC using an f-to-2f self-referencing technique [4].

Advanced systems for mid-IR molecular spectroscopy would undoubtedly benefit from the optoelectronic integration prospects offered by complementary metal–oxide–semiconductor (CMOS) technology. There have been a few demonstrations of coherent SC generation from Si-based chips. These were obtained by pumping Si-on-insulator (SOI) [5,6] or Si nitride-on-insulator waveguides [7] in the anomalous dispersion regime, at near-IR wavelengths, reaching coherent SC covering an octave up to 1.9 μm [7] or 2.4 μm thanks to dispersive wave generation [6] However, achieving coherent SC generation in the anomalous dispersion regime, as in those demonstrations, imposes stringent operation conditions in terms of usable waveguide length, pump pulse duration, and peak power. In particular, a strong nonlinear parameter and high peak power (e.g., using sub-100-fs pulses) are required to achieve soliton fission in a waveguide with a length short enough to suppress modulation instability [7], thereby enabling the resulting SC to preserve the coherence of the pump. Most importantly, the flatness of such SC spectra is degraded during the underlying soliton fission process, where the input pulse irreversibly splits into many pulses, forbidding any post-processing technique to recover the pulse integrity or any efficient pulse compression schemes.

By contrast, achieving fully coherent octave-spanning SC with high spectral flatness is possible when pumping waveguides with sub-picosecond pulses in a low all-normal dispersion (ANDi) regime. Such SCs were reported in various fiber platforms, including silica [8–10], silicate soft glass [11,12], chalcogenide [13–16] fibers. However, SC generation in the ANDi regime on a chip has been only achieved in a chalcogenide waveguide [17] without any discussion about the phase coherence properties across the SC spectrum.

In this Letter, we present what we believe to be the first report of coherent SC generation from a waveguide on a Si-based chip operating in the ANDi regime. We demonstrate a mid-IR octave-spanning SC extending between 2.8 and 5.7 μm by pumping air-clad Si-germanium waveguides on a Si substrate (SiGe-on-Si) with 205 fs pulses at around 4 μm. Our measurements are in good agreement with simulations, enabling us to numerically validate the coherence properties of such a SC

across its entire band. Finally, numerical simulations show that this coherent SC can enable pulse compression down to 22 fs, opening new opportunities for fully integrated nonlinear optical systems.

Ge-based, group IV, on-chip platforms have attracted significant attention for nonlinear applications in the mid-IR thanks to the strong nonlinearity and the transparency of Ge across the entire mid-IR band (2–15 μm) [18]. These platforms include Ge-on-SOI [19], Ge-on-Si [18,20], low (<40%) [21,22], and high (>40%) [23] Ge content SiGe-on-Si. Our SiGe-on-Si platform, with around 40% of Ge in the SiGe alloy, offers a good trade-off between nonlinear performances and low propagation loss for the associated waveguides in the mid-IR band [24]. Using this platform, we recently reported SC generation from 3 μm up to 8.5 μm, with high on-chip SC power (>10 mW) [21].

In this current contribution, we designed our waveguides to achieve ANDi at wavelengths just beyond the three-photon absorption limit in $Si_{0.6}Ge_{0.4}$, around 4 μm [25]. We achieved low (<100 ps/nm/km) and relatively flat ANDi, spanning over an octave bandwidth, for air-clad 2.7 μm thick $Si_{0.6}Ge_{0.4}$/Si (see the inset of Fig. 1) with two slightly different widths of 4.25 μm and 5 μm, respectively. As seen in Fig. 1 for the TM polarization, the wider waveguide has a slightly broader flat ANDi but is multimode in contrast to the narrower, single mode waveguide.

The $Si_{0.6}Ge_{0.4}$-on-Si waveguides were fabricated using a standard CMOS manufacturing process. First of all, 2.7 μm thick $Si_{0.6}Ge_{0.4}$ layers were grown *n* top of Si(001) substrates by reduced pressure chemical vapor deposition. Those $Si_{0.6}Ge_{0.4}$ layers were encapsulated by 550 nm thick Si layers, which were thinned down to 50 nm via chemical–mechanical polishing, to have smooth Si top surfaces. Straight waveguides were patterned on 200 mm wafers using deep ultraviolet photolithography. Finally, air-clad ridge waveguides were formed by a deep reactive-ion etching process [26]. The scanning electron microscope image shows vertical and smooth waveguide sidewalls, as in the inset in Fig. 2. We characterized two sets of air-clad $Si_{0.6}Ge_{0.4}$/ Si waveguides with two widths, 4.25 μm and 5.0 μm, called "narrow" and "wide" waveguides in the following.

We characterized the transmission response of our waveguides in both linear and nonlinear regimes using the experimental setup described in Ref. [21]. To measure propagation losses, we used a tunable optical parametric amplifier (OPA) delivering linearly polarized (TM) low power (<3 mW) 7.5 ps pulses with a 1.5 MHz repetition rate. We measured the propagation loss of narrow and wide waveguides at wavelengths between 3 and 5 μm and in the TM mode using the cut-back method and three different lengths (2, 4, and 7 cm). We estimated the coupling loss per facet to be −4.7 dB at 4.15 μm and −4.2 dB at 4 μm for the narrow and wide waveguides, respectively. Figure 2 shows that losses in the 4 to 5 μm wavelength range are around 0.4 dB/cm and 0.3 dB/cm for narrow and wide waveguides, respectively.

We next probed a narrow waveguide (7 cm long) and a wide waveguide (2 cm long) in the nonlinear regime with ∼200 fs pulses at around 4 μm (delivered by a "Miropa-fs" OPA at 63 MHz repetition rate). Pumping the narrow, "single mode" waveguide enabled us to extract the complete set of nonlinear parameters. The wide "multimode" waveguide was used to obtain the broadest SC spectra, thereby pushing the performance of this SiGe ANDi platform. The measured TM polarized spectral transmissions of the arrow waveguide pumped at 4.15 μm with 205 fs pulses are plotted in Fig. 3(b) for different coupled average (peak) power levels up to 22 mW (3.14 kW). The 4.15 μm pump wavelength avoids the CO_2 absorption peak (∼4.2 μm) and minimizes the waveguide nonlinear losses, as it lies just beyond the three-photon absorption threshold around 4 μm [25]. The inset of Fig. 3(b) also indicates the on-chip output power, which is inferred from the measured transmission and the −4.7 dB coupling loss at the output facet, reaching a bright 6 mW SC signal for the 22 mW coupled average power. Several measured spectral transmission curves are plotted in Fig. 4(b) for the wide waveguide pumped at the 4 μm wavelength with 210 fs pulses. Broad SC generation is achieved in the narrow waveguide with a 10 dB bandwidth of 2.2 μm and a 30 dB bandwidth of 2.8 μm at 22 mW coupled average power. The slightly broader ANDi of the wide waveguide enabled the generation of a broader, octave-spanning SC from 2.8 up to 5.7 μm (i.e., a −30 dB bandwidth of 2.9 μm at 40 mW coupled average power). In addition, both experimental SCs exhibit the characteristic features expected in ANDi waveguides, i.e., a relatively smooth and flat spectrum across a very wide bandwidth, in contrast to typical measurements for anomalous dispersion waveguides [21]. These features directly result from the different driving mechanisms of the spectral broadening of sub-picosecond pulses in the ANDi regime, i.e., self-phase modulation and optical-wave breaking.

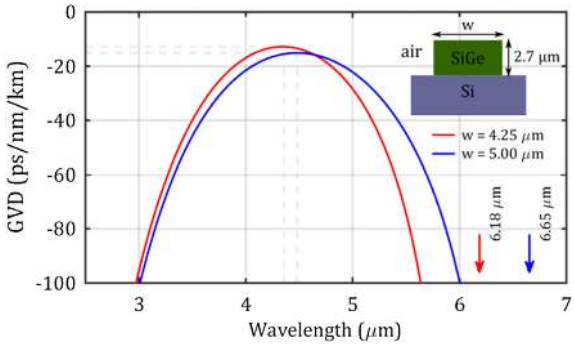

Fig. 1. Calculated group velocity dispersion GVD for 4.25 μm (red) and 5 μm (blue) wide $Si_{0.6}Ge_{0.4}$/Si waveguides. The dashed lines indicate the dispersion peak, and the arrows show the cutoff wavelengths. A schematic of the waveguides is provided in the inset.

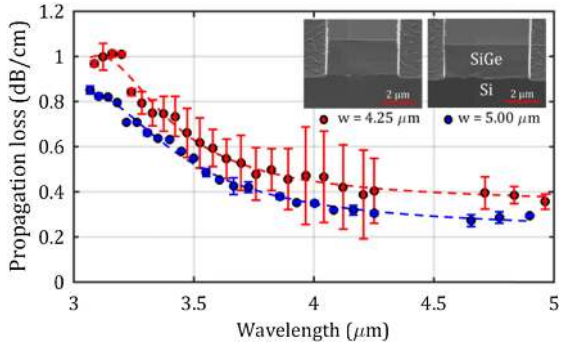

Fig. 2. Measured propagation losses and fits with Lorentzian functions (dashed curves) for 4.25 μm (red) and 5 μm (blue) wide, 2.7 μm thick SiGe/Si air-clad waveguides. The insets show scanning electron microscopy images of the waveguides.

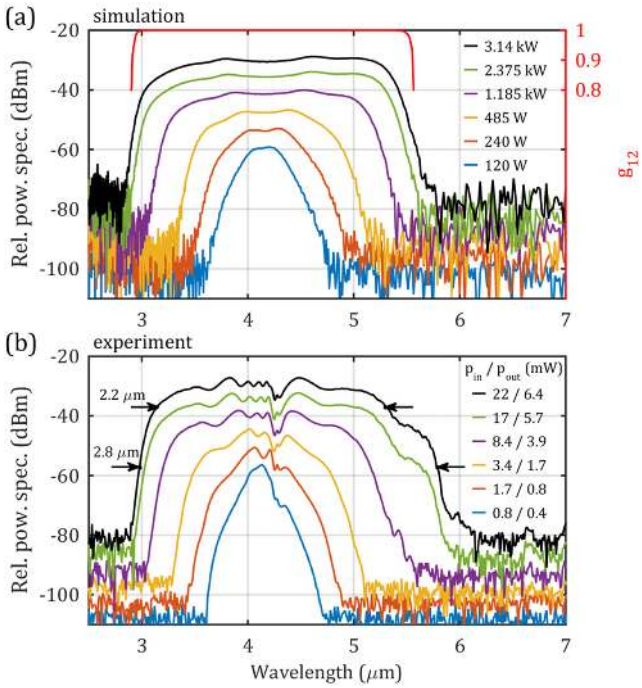

Fig. 3. (a) Simulated and (b) measured SC spectra for the narrow waveguide in the TM polarization for various coupled average powers. The top red curve in (a) shows the SC spectra's calculated coherence at the highest (3.14 kW) peak power. The black arrows in (b) indicate the 10 dB and 30 dB limits of the spectrum. The measured coupled input and on-chip output average powers are given in the inset (b) and the estimated coupled peak powers in the inset (a).

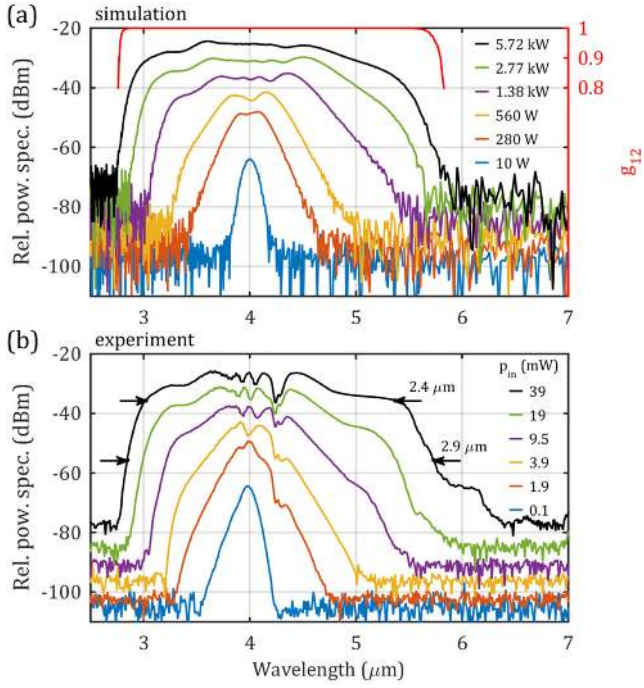

Fig. 4. (a) Simulated and (b) measured SC spectra for the wide waveguide in the TM polarization and various coupled average powers. The top red curve in (a) shows the calculated coherence of the SC spectra at the highest (5.72 kW) peak power. The coupled peak powers and average powers are given in the insets (a) and (b), respectively.

We model the nonlinear pulse propagation in our waveguides by solving the generalized nonlinear Schrodinger equation. The equation includes the nonlinear Kerr effect, four-photon absorption, Raman effects, dispersion, loss, and free-carrier effects. The wavelength dependence of the propagation loss is included by fitting the measured loss with a Lorentzian function (see Fig. 2). The waveguide dispersion is modeled by including dispersion terms up to β_{12}. The dispersion of the nonlinearity is also taken into account, as in Ref. [27], assuming a linear increase of the effective refractive index and the effective area. The Raman response is modeled as in Si waveguides [28].

The first-order coherence degree, $g_{12}^{(1)}$, of the simulated SC is calculated with the following formula [27]:

$$\left|g_{12}^{(1)}(\lambda)\right| = \left|\frac{\langle E_1^*(\lambda)E_2(\lambda)\rangle}{\sqrt{\langle|E_1(\lambda)|^2\rangle\langle|E_2(\lambda)|^2\rangle}}\right|, \quad (1)$$

where angular brackets denote an ensemble average over fifty independently generated pairs of SCs, $E_{1,2}(\lambda)$, with random input noise. Noise was modeled by adding one photon per mode, according to our pump repetition rate $f_r = 63$ MHz, with a Gaussian distribution of both amplitude and phase of variance 2σ equal to $h\nu/2$ and π, respectively [29].

The simulated spectra are plotted for the narrow waveguide in Fig. 3(a), with extremely flat and smooth spectra, again a signature of the ANDi regime. We had the best agreement between experiments [Fig. 3(b)] and simulations with a Kerr index $n_2 = 4.0 \times 10^{-18}$ m^2/W and a four-photon absorption $\alpha_{4PA} = 1.16 \times 10^{-42}$ m^5/W^3 at 4.15 μm ($\gamma = 0.8$ W^{-1} m^{-1}). Fitting the transmission spectra of this single mode waveguide yielded reliable nonlinear parameters, which were tested for the wide, multimode waveguide. The corresponding simulated spectra are shown in Fig. 4(a) for the wide waveguide and the same material parameters. The agreement with measured spectra [Fig. 4(b)] was good. For both waveguides, a small discrepancy is observed in the red part of the spectra, which is most likely due to water vapor absorption at around 5.5–6 μm [30]. In addition, some slight discrepancies in the spectral shape might be due to the modeling of the slightly asymmetric input pulse (see low power spectrum in Fig. 4). From simulations, we inferred a 15 mW on-chip output power from the 2 cm long wide waveguide at 40 mW coupled average power.

The degree of coherence calculated from the simulated spectra at the largest input power is shown for narrow and wide waveguides in Figs. 3(a) and 4(a), respectively. Those figures confirm that the spectra are fully coherent across the entire SC band.

To further illustrate the advantages of generating SC in the ANDi regime, we show in Fig. 5 the simulated spectrograms of the input pulse, the numerically generated SC at the waveguide output, and the compressed pulse after numerically compensating the second- and third-order dispersion for the narrow waveguide (top figures) and the wide waveguide (bottom figures). Pulse compression by second- and third-order dispersion compensation can, in principle, be implemented on-chip by using arrayed-waveguide gratings [26,31]. Our simulations show that it is possible, in principle, to exploit our SC to compress the pump pulses by factors of 3.5 to 9.3, yielding 60 and 22 fs for the narrow and wide waveguides, respectively [see Figs. 5(c) and 5(f)]. More generally, the capability to preserve

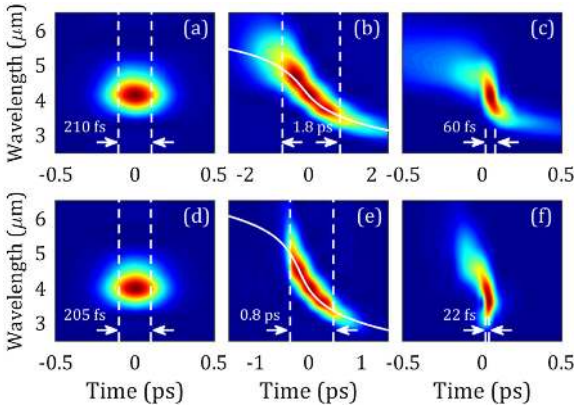

Fig. 5. Simulated pulse spectrograms for the narrow (top) and the wide (bottom) waveguides at the input (left), generated SC at the output (middle), and compressed SC (right) at the highest 4 kW peak pump. The white dashed lines give FWHM pulse durations.

the pulse integrity in the time domain stems from the physical processes under pinning ANDi SC. The maintenance of high quality pulses with on-chip SC generation and pulse compression could enable compression of picosecond pulses from an on-chip mode-locked laser to femtosecond pulses. As the latter are required for octave-spanning coherent SC generation but have remained elusive from on-chip lasers so far, a two stage fully integrated architecture (including the pump) to first compress the pulse could be envisaged to benefit from very broad SC on a chip.

In conclusion, we demonstrated a mid-IR octave-spanning SC in ANDi SiGe-on-Si waveguides. Good agreement was found between measurements and simulations, enabling us to numerically confirm the coherence of the generated SC across its entire bandwidth, from 2.8 up to 5.7 μm. The waveguide dispersion was engineered to exhibit low ANDi across a wide band. The broad spectra generated in this regime were smooth and flat, with a high power spectral density. The fully coherent SC that is generated in this regime lends itself to efficient on-chip pulse compression schemes. It should enable us, in principle, to obtain 22 fs pulses from 205 fs pump pulses. Such chip-based, fully coherent SC sources can enable many useful applications such as optical coherence tomography (OCT) and coherent anti-Stokes Raman spectroscopy (CARS) to be conducted in a robust and highly deployable format.

Funding. H2020 European Research Council (648546); Agence Nationale de la Recherche (ANR-17-CE24-0028).

Acknowledgment. We acknowledge the support of the International Associated Laboratory between France and Australia (LIA ALPhFA).

Disclosures. The authors declare no conflicts of interest.

REFERENCES

1. A. Schliesser, N. Picqué, and T. W. Hänsch, Nat. Photonics **6**, 440 (2012).
2. I. Coddington, N. Newbury, and W. Swann, Optica **3**, 414 (2016).
3. N. Nader, D. L. Maser, F. C. Cruz, A. Kowligy, H. Timmers, J. Chiles, C. Fredrick, D. A. Westly, S. W. Nam, R. P. Mirin, J. M. Shainline, and S. Diddams, APL Photon. **3**, 036102 (2018).
4. M. Sinobad, A. Della Torre, R. Armand, B. Luther-Davies, P. Ma, S. Madden, A. Mitchell, D. J. Moss, J.-M. Hartmann, J.-M. Fedeli, C. Monat, and C. Grillet, IEEE J. Sel. Top. Quantum Electron. **26**, 1 (2020).
5. F. Leo, S. P. Gorza, S. Coen, B. Kuyken, and G. Roelkens, Opt. Lett. **40**, 123 (2015).
6. N. Singh, M. Xin, D. Vermeulen, K. Shtyrkova, N. Li, P. T. Callahan, E. S. Magden, A. Ruocco, N. Fahrenkopf, C. Baiocco, B. P.-P. Kuo, S. Radic, E. Ippen, F. X. Kärtner, and M. R. Watts, Light Sci. Appl. **7**, 17131 (2018).
7. A. R. Johnson, A. S. Mayer, A. Klenner, K. Luke, E. S. Lamb, M. R. Lamont, C. Joshi, Y. Okawachi, F. W. Wise, M. Lipson, U. Keller, and A. L. Gaeta, Opt. Lett. **40**, 5117 (2015).
8. N. Nishizawa and J. Takayanagi, J. Opt. Soc. Am. B **24**, 1786 (2007).
9. A. M. Heidt, A. Hartung, G. W. Bosman, P. Krok, E. G. Rohwer, H. Schwoerer, and H. Bartelt, Opt. Express **19**, 3775 (2011).
10. L. E. Hooper, P. J. Mosley, A. C. Muir, W. J. Wadsworth, and J. C. Knight, Opt. Express **19**, 4902 (2011).
11. M. Klimczak, B. Siwicki, P. Skibinski, D. Pysz, R. Stepien, A. M. Heidt, C. Radzewicz, and R. Buczyński, Opt. Express **22**, 18824 (2014).
12. C. Huang, M. Liao, W. Bi, X. Li, L. Wang, T. Xue, L. Zhang, D. Chen, L. Hu, Y. Fang, and W. Gao, Opt. Lett. **43**, 486 (2018).
13. A. Al-Kadry, L. Li, M. El Amraoui, T. North, Y. Messaddeq, and M. Rochette, Opt. Lett. **40**, 4687 (2015).
14. S. Xing, S. Kharitonov, J. Hu, and C.-S. Brès, Opt. Express **26**, 19627 (2018).
15. H. P. T. Nguyen, T. H. Tuan, L. Xing, M. Matsumoto, G. Sakai, T. Suzuki, and Y. Ohishi, Opt. Express **28**, 17539 (2020).
16. K. Jiao, J. Yao, Z. Zhao, X. Wang, N. Si, X. Wang, P. Chen, Z. Xue, Y. Tian, B. Zhang, P. Zhang, S. Dai, Q. Nie, and R. Wang, Opt. Express **27**, 2036 (2019).
17. Y. Yu, X. Gai, P. Ma, K. Vu, Z. Yang, R. Wang, D.-Y. Choi, S. Madden, and B. Luther-Davies, Opt. Lett. **41**, 958 (2016).
18. G. Z. Mashanovich, C. J. Mitchell, J. S. Penades, A. Z. Khokhar, C. G. Littlejohns, W. Cao, Z. Qu, S. Stanković, F. Y. Gardes, T. B. Masaud, H. M. H. Chong, V. Mittal, G. S. Murugan, J. S. Wilkinson, A. C. Peacock, and M. Nedeljkovic, J. Lightwave Technol. **35**, 624 (2017).
19. S. Radosavljevic, B. Kuyken, and G. Roelkens, Opt. Express **25**, 19034 (2017).
20. M. Nedeljkovic, J. S. Penades, V. Mittal, G. S. Murugan, A. Z. Khokhar, C. Littlejohns, L. G. Carpenter, C. B. E. Gawith, J. S. Wilkinson, and G. Z. Mashanovich, Opt. Express **25**, 27431 (2017).
21. M. Sinobad, C. Monat, B. Luther-Davies, P. Ma, S. Madden, D. J. Moss, A. Mitchell, D. Allioux, R. Orobtchouk, S. Boutami, J.-M. Hartmann, J.-M. Fedeli, and C. Grillet, Optica **5**, 360 (2018).
22. M. Sinobad, A. Della Torre, B. Luther-Davis, P. Ma, S. Madden, S. Debbarma, K. Vu, D. J. Moss, A. Mitchell, J.-M. Hartmann, J.-M. Fedeli, C. Monat, and C. Grillet, J. Opt. Soc. Am. B **36**, A98 (2019).
23. D. Marris-Morini, V. Vakarin, J. M. Ramirez, Q. Liu, A. Ballabio, J. Frigerio, M. M. Ballester, C. Alonso-Ramos, L. R. Xavier, S. Serna, D. Benedikovič, D. Chrastina, L. Vivien, and G. Isella, Nanophotonics **7**, 1781 (2018).
24. L. Carletti, M. Sinobad, P. Ma, Y. Yu, D. Allioux, R. Orobtchouk, M. Brun, S. Ortiz, P. Labeye, J. M. Hartmann, S. Nicoletti, S. Madden, B. Luther-Davies, D. J. Moss, C. Monat, and C. Grillet, Opt. Express **23**, 32202 (2015).
25. N. K. Hon, R. Soref, and B. Jalali, J. Appl. Phys. **110**, 11301 (2011).
26. J. Fedeli and S. Nicoletti, Proc. IEEE **106**, 2302 (2018).
27. J. M. Dudley, G. Genty, and S. Coen, Rev. Mod. Phys. **78**, 1135 (2006).
28. L. Yin, Q. Lin, and G. P. Agrawal, Opt. Lett. **32**, 391 (2007).
29. A. Ruehl, M. J. Martin, K. C. Cossel, L. Chen, H. McKay, B. Thomas, C. Benko, L. Dong, J. M. Dudley, M. E. Fermann, I. Hartl, and J. Ye, Phys. Rev. A **84**, 011806 (2011).
30. P. Linstrom, *NIST Chemistry Webbook, SRD 69* (National Institute of Standards and Technology, 1997).
31. H. Tsuda, K. Okamoto, T. Ishii, K. Naganuma, Y. Inoue, H. Takenouchi, and T. Kurokawa, IEEE Photon. Technol. Lett. **11**, 569 (1999).